Interstitial transition atom impurities in silicon: electronic structure and lattice relaxation

1984 J. Phys. C: Solid State Phys. 17 6047

(http://iopscience.iop.org/0022-3719/17/34/007)

J. Phys. C: Solid State Phys., 17 (1984) 6047–6062. Printed in Great Britain

Interstitial transition atom impurities in silicon: electronic structure and lattice relaxation

U Lindefelt† and Alex Zunger‡
† Department of Theoretical Physics, University of Lund, Sölvegatan 14A, S-223 62 Lund, Sweden
‡ Solar Energy Research Institute, Golden, Colorado 80401, USA

Received 3 July 1984

Abstract. Both the electronic structure and the 'breathing-mode' relaxation for tetrahedral interstitial 3d transition atom impurities in silicon are studied in the local-density approximation. The calculations show that although the interstitial 3d impurities constitute a very large perturbation locally, they interact rather weakly with the surrounding crystal in the sense that they perturb the spatial distribution of electrons on the surrounding atoms only weakly. A special pattern of relaxation is predicted, with an outward relaxation of the first-nearest neighbours and an inward relaxation of the second-nearest neighbours. It is explained in terms of the impurity-induced charge rearrangement.

1. Introduction

Isolated 3d transition atom impurities in semiconductors are among the most difficult point defects that can be studied theoretically. Unlike simple sp-bonded impurities (for instance intrinsic point defects), the localised but chemically and electrically active d-electrons give rise to effects which are still lacking a proper *a priori* description. A lot of data suggest that the 3d electrons occupy partially filled shells and are atomic-like in their localisation, leading to multiplet splitting and a net spin obeying Hund's rules (Ludwig and Woodbury 1962, Kaufmann and Schneider 1980). Thus, a detailed description of these systems generally requires a treatment of the electron–electron interaction that goes beyond the one-particle (mean-field) theory. On the other hand, there have been observed g-factors, intra-atomic (d–d) transition energies and ionisation energies which are reduced considerably compared with the free-ion values, indicating that the wavefunctions still hybridise substantially with the surrounding matrix of atoms and become delocalised.

Density-functional theory has proved very useful as a tool for gaining insight into the electronic structure of atoms, molecules and solids in general. Because of the tendency of atomic states to delocalise in the solid, one expects the local-density theory to give a reasonable, on-the-average description also of the electronic structure of 3d impurities in semiconductors. In this paper the full consequences of this assumption are studied: we report a self-consistent calculation on tetrahedral interstitial 3d transition atom impurities in silicon within the local-density approximation, and predict the

0022-3719/84/346047 + 16 $02.25

'breathing-mode' relaxation of the surrounding lattice. Electron paramagnetic resonance (EPR) studies suggest (Ludwig and Woodbury 1962, Weber 1983) that most transition atom impurities in silicon occupy the tetrahedral interstitial (TI) site, *preserving* the T_d symmetry of the host crystal. A brief description of the electronic structure of these systems (without lattice relaxation) has been given earlier (Zunger and Lindefelt 1982). In § 3 of the present paper we give a more detailed account, especially of those features in the electronic structure which govern the lattice relaxation.

Previous calculations on defect-induced relaxation were done mainly on ionic solids (see Stoneham (1982) and references therein). In semiconductor physics, progress in this field has been hampered by the lack of methods for performing reliable electronic structure calculations on impurities in extended host semiconductors. Recently, a simple model was proposed for studying the symmetry-conserving relaxation of the lattice (Lindefelt 1983, Lindefelt and Zunger 1984). The input to the model consists of the impurity-induced change in charge density before relaxation, which can be obtained to a very high degree of accuracy from the quasi-band crystal-field (QBCF) method (Lindefelt and Zunger 1982). The relaxation model is briefly reviewed in § 2, and its applicability is discussed. Apart from the simplicity, one of its main advantages compared with, for instance, total-energy calculations is that the physical mechanism behind the relaxation is easily analysed and clarified. In § 4 we use this model and predict the pattern of relaxation for the impurities Cr, Mn, Fe, Co and Ni in the 3d series, and relate this to the results of the electronic structure calculations. In short, this paper represents an attempt to give, within the local-density approximation, a unified account of the electronic structure and symmetric lattice relaxation of tetrahedral interstitial 3d impurities in silicon.

2. The relaxation model and its accuracy

Consider a host crystal containing N atoms in their equilibrium positions $\boldsymbol{R}_\mu^0$, $\mu = 1, 2, \ldots, N$. If an impurity atom is introduced at the TI position $\boldsymbol{R}_I$, then the host atoms will in general move to new, distorted equilibrium positions $\boldsymbol{R}_\mu \neq \boldsymbol{R}_\mu^0$. Choosing arbitrarily $\boldsymbol{R}_I = 0$, the atomic positions in the defect crystal and in the host crystal are described by the $3N$-dimensional vectors

$$\boldsymbol{Q} = (\boldsymbol{R}_1, \boldsymbol{R}_2, \ldots, \boldsymbol{R}_N) \qquad \boldsymbol{Q}^0 = (\boldsymbol{R}_1^0, \boldsymbol{R}_2^0, \ldots, \boldsymbol{R}_N^0), \tag{1}$$

respectively. The new position vectors $\boldsymbol{R}_\mu$ are those which minimise the total energy, E, of the system, which, in the density-functional theory, can be written

$$E = E[\rho(\boldsymbol{r}, \boldsymbol{Q}), \boldsymbol{Q}], \tag{2}$$

where $\rho(\boldsymbol{r}, \boldsymbol{Q})$ denotes the total charge density. For an arbitrary vector $\boldsymbol{Q}$ one can define the quantum-mechanical force

$$\boldsymbol{F}_p(\boldsymbol{Q}) = -\nabla_p E[\rho(\boldsymbol{r}, \boldsymbol{Q}), \boldsymbol{Q}]. \tag{3}$$

With an all-electron charge density, $\boldsymbol{F}_p(\boldsymbol{Q})$ will be the force acting on the *nucleus* of the pth atom, whereas for a pseudo-charge density, $\boldsymbol{F}_p(\boldsymbol{Q})$ represents the force acting on the pth (pseudo) *ion*. Using local host atom pseudopotentials and the electrostatic

Hellmann–Feynman (HF) theorem, the force acting on the pth host ion is then given by

$$\boldsymbol{F}_p(\boldsymbol{Q}) = \int (-\nabla_p v_{ps}(|\boldsymbol{r} - \boldsymbol{R}_p|))\rho(\boldsymbol{r}, \boldsymbol{Q})\mathrm{d}^3\boldsymbol{r} + \sum_{\mu \neq p} \frac{z_p^{\mathrm{H}} z_\mu^{\mathrm{H}}}{|\boldsymbol{R}_p - \boldsymbol{R}_\mu|^3}(\boldsymbol{R}_p - \boldsymbol{R}_\mu) + \frac{z_p^{\mathrm{H}} z^{\mathrm{I}}}{|\boldsymbol{R}_p - \boldsymbol{R}_{\mathrm{I}}|^3}(\boldsymbol{R}_p - \boldsymbol{R}_{\mathrm{I}}), \tag{4}$$

where z_μ^{H} denotes the valence of the host atom at site $\boldsymbol{R}_\mu$ and z^{I} the valence of the interstitial impurity atom. The reason for working in the pseudopotential picture is twofold: (i) it simplifies the calculation of ρ considerably and (ii) the errors in the force when calculated with the HF theorem, which are caused by errors in ρ, are generally much smaller in the pseudopotential case than in the all-electron case (Harris *et al* 1981).

Next we split up the total pseudo charge density according to

$$\rho(\boldsymbol{r}, \boldsymbol{Q}) = \rho^{\mathrm{H}}(\boldsymbol{r}, \boldsymbol{Q}) + \Delta\rho(\boldsymbol{r}, \boldsymbol{Q}), \tag{5}$$

where ρ^{H} denotes the charge density in the (impurity-free) host crystal and $\Delta\rho$ the change in charge density caused by the impurity. We can further split up each term in equation (5) to isolate the dependence on relaxation:

$$\rho(\boldsymbol{r}, \boldsymbol{Q}) = \rho^{\mathrm{H}}(\boldsymbol{r}, \boldsymbol{Q}^0) + \delta\rho^{\mathrm{H}}(\boldsymbol{r}, \boldsymbol{Q} - \boldsymbol{Q}^0) + \Delta\rho(\boldsymbol{r}, \boldsymbol{Q}^0) + \delta\Delta\rho(\boldsymbol{r}, \boldsymbol{Q} - \boldsymbol{Q}^0). \tag{6}$$

The first approximation in the model consists of neglecting the term $\delta\Delta\rho(\boldsymbol{r}, \boldsymbol{Q} - \boldsymbol{Q}^0)$. Substituting the resulting expression for $\rho(\boldsymbol{r}, \boldsymbol{Q})$ into the HF theorem, equation (4), gives

$$\boldsymbol{F}_p(\boldsymbol{Q}) = \boldsymbol{F}_p^{\mathrm{H}}(\boldsymbol{Q}) + \Delta\boldsymbol{F}_p(\boldsymbol{Q}). \tag{7}$$

Here the driving force $\Delta\boldsymbol{F}_p(\boldsymbol{Q})$ caused by the impurity is given by

$$\Delta\boldsymbol{F}_p(\boldsymbol{Q}) = \int (-\nabla_p v_{ps}(|\boldsymbol{r} - \boldsymbol{R}_p|))\Delta\rho(\boldsymbol{r}, \boldsymbol{Q}^0)\mathrm{d}^3\boldsymbol{r} + \frac{z_p^{\mathrm{H}} z^{\mathrm{I}}}{|\boldsymbol{R}_p - \boldsymbol{R}_{\mathrm{I}}|^3}(\boldsymbol{R}_p - \boldsymbol{R}_{\mathrm{I}}) \tag{8}$$

while $\boldsymbol{F}_p^{\mathrm{H}}(\boldsymbol{Q})$ is easily seen to be the restoring force from the host crystal. The second approximation consists of calculating the restoring force, not from the HF theorem, but from an empirical valence force (VF) model:

$$\boldsymbol{F}_p^{\mathrm{H}}(\boldsymbol{Q}) = -\nabla_p \Phi(\boldsymbol{Q}), \tag{9}$$

where $\Phi(\boldsymbol{Q})$ is the potential energy of the vibrational motion. This can be determined by fitting an appropriate analytical expression to experimental phonon spectra for the host crystal, and has been done for silicon (Solbrig 1971, Larkins and Stoneham 1971a, b, Lindefelt 1983).

For the purpose of analysing the way in which $\Delta\rho(\boldsymbol{r}, \boldsymbol{Q}^0)$ affects the driving force, it is convenient to make a change of origin of the integrand in equation (8) and introduce the density fluctuation relative to the pth host atom:

$$\Delta n^{(p)}(\boldsymbol{r}) = \Delta\rho(\boldsymbol{r} + \boldsymbol{R}_p) \tag{10}$$

where we have used the abbreviated notation $\Delta\rho(\boldsymbol{r}) = \Delta\rho(\boldsymbol{r}, \boldsymbol{Q}^0)$ for the impurity-centred change in charge density. Each function $\Delta n^{(p)}(\boldsymbol{r})$ can be expanded in a Kubic harmonics series,

$$\Delta n^{(p)}(\boldsymbol{r}) = \sum_{l=0}^{\infty} \sum_{\alpha, \lambda} \Delta n_{l, \alpha, \lambda}^{(p)}(r) K_l^{\alpha, \lambda}(\hat{\boldsymbol{r}}) \tag{11}$$

where $K_l^{\alpha\lambda}(\hat{r})$ denotes a Kubic harmonic of order l transforming as the λth partner in the αth irreducible representation of the group T_d. If we define the $l = 1$ projection $\boldsymbol{n}^{(p)}(r)$ of the charge-density perturbation around the pth atomic site as a three-component vector function

$$\boldsymbol{n}^{(p)}(r) = -(4\pi/3)^{1/2}(\Delta n^{(p)}_{1,t_2,x}(r), \Delta n^{(p)}_{1,t_2,y}(r), \Delta n^{(p)}_{1,t_2,z}(r)), \tag{12}$$

where x, y and z label the three partners in the irreducible representation t_2, equation (8) can be written rigorously as

$$\Delta \boldsymbol{F}_p(\boldsymbol{Q}) = \int \left(-r^2 \frac{\mathrm{d}v_{ps}(r)}{\mathrm{d}r} \right) \boldsymbol{n}^{(p)}(r)\,\mathrm{d}r + \frac{z_p^{\mathrm{H}} z^{\mathrm{I}}}{|\boldsymbol{R}_p - \boldsymbol{R}_{\mathrm{I}}|^3}(\boldsymbol{R}_p - \boldsymbol{R}_{\mathrm{I}}). \tag{13}$$

Thus, only the $l = 1$ term in the Kubic harmonic expansion of $\Delta\rho(\boldsymbol{r})$ around the pth atomic site in equation (11) contributes to the driving force. This makes it possible to examine rather easily how details in $\Delta\rho(\boldsymbol{r})$ influence the driving force and hence the relaxation.

In order to examine the nature of the approximations in the relaxation model, we note first of all that, since the approximations concern only the $\boldsymbol{Q}$-dependence in $\rho(\boldsymbol{r}, \boldsymbol{Q})$ (i.e. the value of $\rho(\boldsymbol{r}, \boldsymbol{Q})$ for $\boldsymbol{Q} \neq \boldsymbol{Q}^0$), they will not affect the predicted direction of distortion, only the amount by which the atoms are displaced. Secondly, we observe that the use of the VF model for the restoring forces, which was obtained by fitting to experimental phonon spectra, presumably limits the model to small distortions, but, to within the limitations of the VF model, the effect on the forces from the host charge density $\rho^{\mathrm{H}}(\boldsymbol{r}, \boldsymbol{Q})$ is in principle treated with its full $\boldsymbol{Q}$ dependence. It is then clear that as long as we do not question the validity of the VF model, the *basic approximation* in the relaxation model is that *the $\boldsymbol{Q}$ dependence in $\rho(\boldsymbol{r}, \boldsymbol{Q})$ is approximated by the $\boldsymbol{Q}$ dependence in $\rho^{\mathrm{H}}(\boldsymbol{r}, \boldsymbol{Q})$*. Thus, for substitutional impurities, the relaxation model is expected to give accurate results for the magnitude of the distortion when the impurity atom is not too different from the atom it replaces. This indicates, for instance, that the relaxation model should be more accurate for substitutional Si : S than for the vacancy.

For interstitial defects, it is more difficult to give a similar rule of thumb. We observe, however, that around the TI position, the host charge density is very low, while, at the same time, stable bonds between the host atoms, away from the interstitial site, already exist. One would therefore in general expect that impurities in the TI position interact weakly with the host. As a matter of fact, it will be seen later (§ 3) that this is indeed the case. Therefore, in the neighbourhood of the TI position, both $\rho^{\mathrm{H}}(\boldsymbol{r}, \boldsymbol{Q})$ and $\Delta\rho(\boldsymbol{r}, \boldsymbol{Q})$ should be rather insensitive to the exact positions of the surrounding atoms. Since, furthermore, the displacement of the nearest shells of atoms turns out to be quite small in these systems (typically around 4% of a Si–Si bond length), the lowest term neglected in the $\boldsymbol{Q}$ dependence in $\rho(\boldsymbol{r}, \boldsymbol{Q})$, i.e.

$$(\boldsymbol{Q} - \boldsymbol{Q}^0) \cdot \frac{\partial \Delta\rho(\boldsymbol{r}, \boldsymbol{Q})}{\partial \boldsymbol{Q}} \tag{14}$$

is expected to be of minor importance.

Although it is difficult to give a good quantitative estimate of the absolute errors in the predicted distortions, it is possible to give a simple argument why the predicted *trends* for a series of impurities should be correctly described by the model. We will see later (§ 4) that there is always a one-to-one correspondence between the strength of the forces on the *undistorted* atoms (referred to as the initial forces), and the distance by

which they are displaced: the larger the initial force is on a given atom, the more it is displaced. This feature is reasonable, especially since the distortions are small. The initial forces are, of course, not affected by the two approximations in the relaxation model, but their chemical trends depend only on the *relative* accuracy by which $\Delta\rho(\boldsymbol{r})$ can be calculated, which is very high in the QBCF method.

3. Some results from the electronic structure calculations

In this section we shall give a brief description of some of the main results from the self-consistent electronic structure calculations on TI Cr, Mn, Fe, Co and Ni impurities in silicon (point symmetry group T_d). The calculations are self-consistent within the pseudopotential local-density approximation with Slater's exchange parameter $\alpha = 1.0$. For the silicon host atom we employed the local semi-empirical pseudopotential of Louie *et al* (1976), and for the impurity atoms we have used the first-principles non-local atomic pseudopotentials of Zunger and Cohen (1978, 1979).

In the QBCF method (for full details, see Lindefelt and Zunger 1982), all wavefunctions are expanded in a crystal-field-like manner:

$$\psi_i^{\alpha\lambda}(\boldsymbol{r}) = \sum_l G_{il}^{\alpha}(r) K_l^{\alpha\lambda}(\hat{\boldsymbol{r}}). \tag{15}$$

Here the subscript i denotes a particular one-particle state. The radial functions $G_{il}^{\alpha}(r)$ are expressed in terms of some conveniently chosen set of basis functions $\{F_{\mu l}(r)\}$ (usually a mixture of Coulombic and atomic wavefunctions):

$$G_{il}^{\alpha}(r) = \sum_{\mu} C_{\mu li}^{\alpha} F_{\mu l}(r), \tag{16}$$

where the expansion coefficients are determined numerically. The expansion in equation (15) is required to hold only in the central cell (CC) region, i.e. in a sphere centred at the impurity site and with a radius R_{CC} extending out to the nearest-neighbour host atoms. In silicon $R_{CC} = 4.44$ au both for the substitutional and tetrahedral interstitial sites. As a measure of the amount of localisation for a particular state $|i\rangle$ we use the quantity

$$q_i \equiv \int_{CC} |\psi_i^{\alpha\lambda}(\boldsymbol{r})|^2 \, \mathrm{d}^3\boldsymbol{r} = \sum_l \int_0^{R_{CC}} (G_{il}^{\alpha}(r))^2 r^2 \, \mathrm{d}r \tag{17}$$

Each term in equation (17), denoted q_{il}, i.e.

$$q_{il} = \int_0^{R_{CC}} (G_{il}^{\alpha}(r))^2 r^2 \, \mathrm{d}r, \tag{18}$$

is then a measure of the degree of l-character in the wavefunction within the CC. Furthermore, equation (15) leads naturally to the very convenient, impurity-centred expansion

$$\Delta\rho(\boldsymbol{r}) = \sum_l \Delta\rho_l(r) K_l^{a_1}(\hat{\boldsymbol{r}}) \tag{19}$$

of the defect-induced change in charge density inside the CC, and, of course, to a similar expression for the total charge density $\rho(\boldsymbol{r})$. In equation (19), a_1 denotes the totally symmetric representation in T_d. The explicit expression for the three lowest $K_l^{a_1}(\hat{\boldsymbol{r}})$ are,

in cartesian coordinates,

$$K_0^{a_1}(\hat{r}) = (4\pi)^{-1/2} \qquad K_3^{a_1}(\hat{r}) = (105/4\pi)^{1/2}xyz/r^3$$
$$K_4^{a_1}(\hat{r}) = (21/16\pi)^{1/2}[3(x^2y^2 + x^2z^2 + y^2z^2) - (x^4 + y^4 + z^4)]/r^4. \qquad (20)$$

Because of the high symmetry, the only non-zero l-components compatible with the a_1 representation in T_d are $l = 0, 3, 4, 6, 7, 8$ etc. In most cases, the defect gives rise to partially occupied states. When this happens, the charge density contains, in principle, components with symmetry lower than a_1 together with the a_1-symmetric component in equation (19). However, in mean-field calculations the charge density is a_1-symmetrised, i.e. only the a_1-symmetric component of $\Delta\rho(r)$ is retained (cf mean-field atomic calculations where the charge density is spherically symmetrised). This is achieved by populating each of the partner functions of the partially occupied states by equal amounts of electronic charge. We shall follow this conventional procedure here.

The defect energy levels introduced into the band gap by the neutral impurities are shown in figure 1. The occupation numbers (in parentheses) have been chosen to be consistent with observed EPR data (Ludwig and Woodbury 1962), i.e. to favour high-spin states. We see that Ni is predicted to be electrically inactive in the ground state since there are no partially filled gap states, and that for Co and Fe only the one-particle levels of e symmetry are electrically active. Furthermore, the crystal-field splitting of the gap states, defined as the energy separation between the bound e and t_2 states, increases slightly towards the lighter end of the series, reflecting a decreasing localisation of the corresponding wavefunctions. Actually it is the gap states of e symmetry that become more delocalised for the lighter elements ($q_e = 0.58, 0.55, 0.44$ and 0.23 for Co, Fe, Mn and Cr, respectively) whereas the t_2 gap states have roughly the same localisation ($q_{t_2} = 0.36$ for Mn and 0.38 for Cr). As to the amount of d character in the gap-state wavefunctions inside the CC (measured by q_{il}/q_i for i = gap and $l = 2$), we find that the e states have almost 100% d character and that the t_2 states have more than 90% d character. As an example of a wavefunction we show in figure 2 the gap-state wavefunction of e symmetry for Si:Fe in the $\pm\langle 1, 1, 0\rangle$ crystal directions. The shaded area

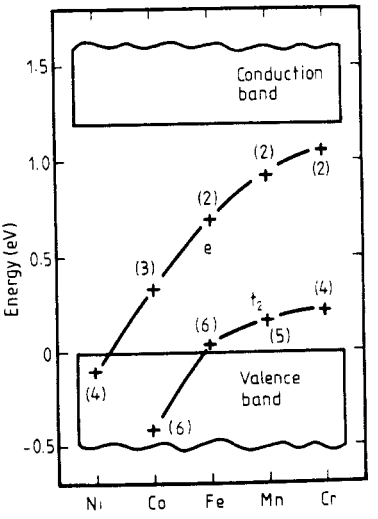

Figure 1. Defect energy levels around the band gap introduced by TI 3d impurities in silicon. The numbers in parentheses are the occupation numbers.

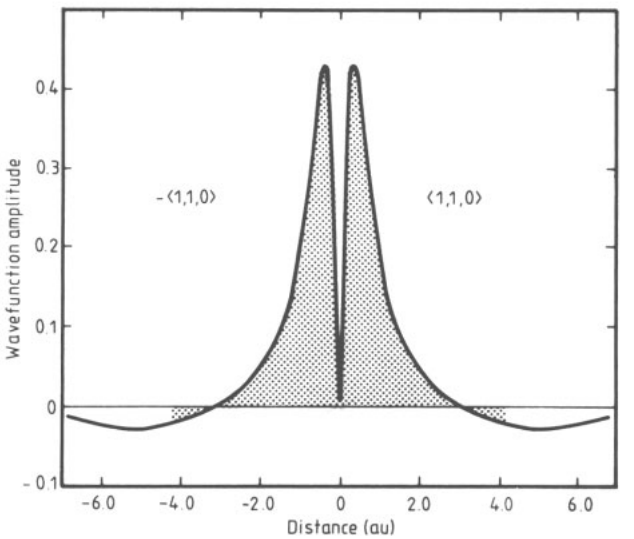

Figure 2. Bound-state wavefunction of e symmetry for Si:Fe in the $\pm\langle 1, 1, 0\rangle$ directions. The shaded area corresponds to 50% of the normalisation integral.

indicates the part of the wavefunction which corresponds to around 50% of the normalisation integral. The wavefunction is clearly very atomic-like in the inner CC (almost 100% atomic d character as mentioned earlier), but with an amplitude that, inside the core, is reduced by a factor 0.7 compared with the free atom. Around 50% of the wavefunction must thus reside outside the CC, where its amplitude is seen to be relatively small. This indicates that the wavefunction can be regarded as being rather delocalised, with a large atomic-like peak near the origin. It can therefore be expected that this state shows features which are characteristic for both localised states, e.g. multiplet splitting, hyperfine interaction, and delocalised states, e.g. many charged states in a narrow energy region, like the band gap, and reduced g-factors. Both these features have been observed experimentally, as mentioned in the Introduction.

Even though the gap-state wavefunctions of, for instance, e symmetry typically have as much as 50% of their total charge outside the CC, $\Delta\rho(\boldsymbol{r})$ is nevertheless essentially localised within this region of space. This is illustrated in figures 3 and 4 for Si:Fe. Figure 3 shows the spherically symmetric component $\Delta\rho_0(r)$ of (the impurity-centred) $\Delta\rho(\boldsymbol{r})$, and in figure 3($a$) the anisotropic component $\Delta\rho_4(r)$ is also shown. At first sight, there is a surprisingly large anisotropy in $\Delta\rho(\boldsymbol{r})$ close to the Fe nucleus. The reason is that in a mean-field calculation of the charge density for the free 3d atom, the $l = 4$ component of the charge density for the atomic 3e state cancels that of the atomic $3t_2$ state to produce a spherically symmetric charge density, because (i) the two states have the same radial function and (ii) the occupancy of the e state (n_e) relative to the dimension of the e representation (d_e) is the same as for the t_2 state, i.e. $n_e/d_e = n_{t_2}/d_{t_2}$. In the solid, however, we have for Fe $n_e/d_e = 1$ and $n_{t_2}/d_{t_2} = 2$. Therefore complete cancellation does not occur, but there is a residual $l = 4$ component of $\Delta\rho(\boldsymbol{r})$ which consists of a product of the sharply peaked $l = 2$ components of the wavefunctions. In the case Si:Ni, the condition (ii) is fulfilled, but the e and t_2 states in figure 1 have somewhat different radial $l = 2$ functions, so that not even in this case does complete cancellation occur, although now the residual $l = 4$ component is much smaller than for the other impurities. In figure

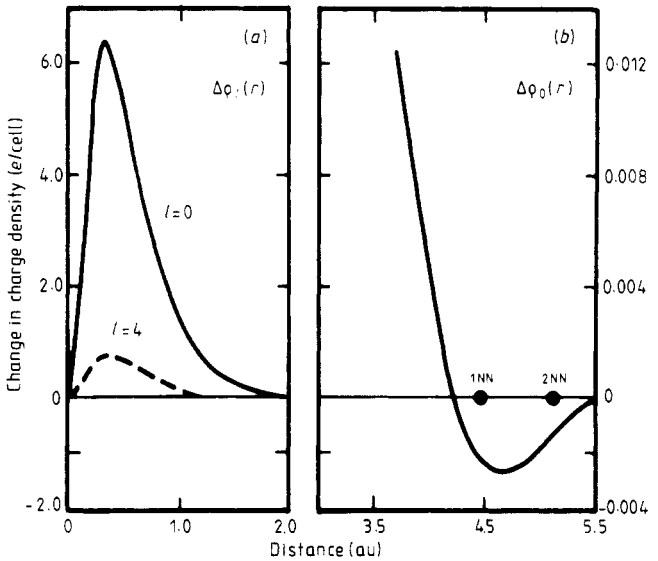

Figure 3. (*a*) Radial components of the change in charge density for Si:Fe. The $l = 3$ component is too small to be seen in this scale. (*b*) Spherically symmetric component of the change in charge density for Si:Fe around the first and second nearest neighbours.

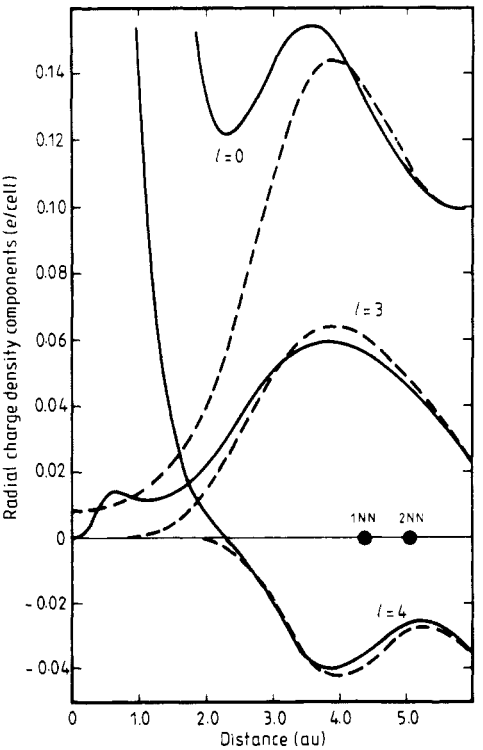

Figure 4. The three lowest l components of the total charge density around the TI position for Si:Fe (full curves) and bulk silicon (broken curves).

4 we show the three lowest radial components of the total charge density $\rho(r)$ (full curves) together with the radial components of the host charge density around the TI site (broken curves). In the direction towards the 1NN at $(a/4)$ (1, 1, 1), where a is the lattice constant, the Kubic harmonics are all positive. Therefore, figure 4 shows that charge has been displaced towards the impurity, mainly through the spherically symmetric component but also through the anisotropic components. In the direction towards the 2NN at $a/2(1, 0, 0)$, $K_3^{a1}(\hat{r}) = 0$ and $K_4^{a1}(\hat{r})$ is negative. The spherical $l = 0$ component again describes the largest displacement of charge towards the impurity, whereas there is an anisotropic depletion of charge through the $l = 4$ component close to the nucleus and a minor depletion of charge also at the 2NN. Except for the peaks in $\Delta\rho_0(r)$ and $\Delta\rho_4(r)$, which are both inside the impurity core, the defect-induced charge rearrangement is seen to be small. In this sense the TI 3d impurities interact weakly with the host, as pointed out in § 2. We can therefore picture an interstitial 3d impurity as being essentially a spherically symmetric cloud of charge, filling out the rather empty region around the tetrahedral interstitial position out to the nearest-neighbour atoms, without affecting the bonds (or the charge distribution in general) in the rest of the crystal. This is to be contrasted to substitutional transition atom impurities and the vacancy (Zunger and Lindefelt 1983) for which again the impurity-induced charge rearrangement is localised to the CC, but where there is a substantial perturbation (weakening) of the bonds due to the deficiency in the number of valence electrons that can repair the broken bonds (Lindefelt 1983).

By analysing the quantities q_{il}, which can also be interpreted as describing how the various l-components of the occupied wavefunctions contribute to the total charge around the impurity (see equations (17) and (18)), we find that when the atomic 3d shell is not completely filled, the atomic 4s electrons go into the 3d shell, i.e. the atomic $d^n s^m$ configuration becomes effectively a $d^{n+m}s^0$ configuration in the solid. This s–d population inversion (Zunger and Lindefelt 1982) compared with the free atom was envisaged already by Ludwig and Woodbury (1962) in their classical model. The s–d population inversion suggests a simple explanation of the high diffusion constant D for Ni in silicon ($D \sim 10^{-4}$ cm^2 s^{-1}) relative to the lighter TA impurities ($D \sim 10^{-8}$ to 10^{-10} cm^2 s^{-1}). In the solid, the Ni atom effectively assumes a closed-shell, noble-atom-like d^{10} configuration. One would therefore expect Ni to diffuse easily through the solid.

4. Impurity-induced symmetric relaxation of the lattice

It is a well known fact that the evaluation of forces using the electrostatic HF theorem requires a highly accurate charge density (see for instance Deb 1973), even though the use of pseudopotentials to a large extent makes this requirement less pronounced, as mentioned earlier. In calculations like those reported here, there are mainly two sources of errors, namely incompleteness of the basis set (cf equation (16)) and departure from self-consistency. The first of these will affect the degree to which a wavefunction is an eigenfunction to the Hamiltonian. Sufficient variational flexibility is achieved by using a very large and impurity-related set (192 s, p, d, f and g functions) of optimised basis functions (Lindefelt and Zunger 1982). The self-consistency requirement should generally be an order of magnitude more stringent than what is needed in electronic structure calculations. In the calculations reported here, the difference between input and output potentials is typically 1–2 mRyd (a difference of about 10 mRyd is usually sufficient to give converged energies). Another input parameter that has to be specified is the number

of atoms around the impurity that are allowed to relax. In these calculations we let the first nine shells around the impurity, corresponding to 82 atoms (or all atoms within a sphere of radius 15 au around the impurity), relax freely while all other atoms are kept in their original positions. We then calculate the equilibrium configuration $\boldsymbol{Q} = \boldsymbol{Q}^*$ of T_d symmetry from the condition that the total force $\boldsymbol{F}_p(\boldsymbol{Q}^*)$ in equation (7) vanishes simultaneously at all 82 sites, corresponding to finding that particular arrangement of atoms which minimises the total energy. This difficult optimisation problem is solved efficiently and elegantly by the Jacobian update method (Lindefelt 1983). The restriction to the fully symmetric (a_1) distortions is imposed by the omission of other components in $\Delta\rho(\boldsymbol{r})$ than those having full T_d symmetry, in accordance with the mean-field theory (§ 3), while symmetry-lowering (Jahn–Teller) distortions necessarily require a charge density of symmetry lower than a_1. From figure 1 it is seen that Ni has no partially occupied states, and therefore these calculations predict that there is no Jahn–Teller distortion induced by the T1 Ni impurity, so the breathing-mode displacements calculated here give the complete distortion. There is also experimental evidence from spin-resonance measurements that the impurities Cr, Mn and Fe in silicon (which are believed to be T1) show no sign of Jahn–Teller distortions (Weber 1983 and private communication).

The results of the calculations of the a_1-symmetric ('breathing-mode') relaxation around the T1 3d impurities in silicon are summarised in figure 5. We observe four shells with a relatively large distortion, containing altogether 26 atoms. The four first-nearest neighbours (1NN), which in their undistorted positions are located at 4.44 au from the T1 site, move away from the impurity. Averaging over the different impurities, we find the averaged outward displacement to be around 0.14 au. For the six atoms in the second shell (2NN), which in the perfect crystal are 5.13 au from the T1 site, the displacement is opposite to that of the first shell, i.e. the atoms move towards the impurity. The averaged inward displacement is in this case around 0.18 au. Thus the distance between the two shells has, on average, decreased from 0.69 au to 0.37 au, i.e. by a factor two, leading to an approximately tenfold-coordinated transition atom. As an interesting comparison, we note that all three metallic bulk disilicide structure types, the $TiSi_2$ (orthorhombic), $CrSi_2$ (hexagonal) and $MoSi_2$ (tetragonal) structures, avoid the conventional close-packing coordination of 12, and assume an approximately tenfold coordination around the transition atom (Wells 1975).

The driving forces caused by the defects are non-zero only on the first two shells of atoms. The contribution to $\Delta\boldsymbol{F}_p$ from $\Delta\rho_0(r)$ is cancelled by the ion–ion repulsion term in equation (8) for atoms outside the range of $\Delta\rho(\boldsymbol{r})$, whereas the driving force due to the anisotropic components of $\Delta\rho(\boldsymbol{r})$ in principle extend to infinity. However, this contribution to the force turns out to be very small on the third shell (at 8.51 au) and beyond. These shells have therefore moved only because of the displacement of the two inner shells. The fourth shell (at 8.9 au) is seen to have a relatively large distortion, which, with respect to the chemical trends, closely follows that of the first shell, appropriately scaled. The reason for this is that each atom in the fourth shell is directly attached to an atom in the first shell with a bond which is pointing along the common direction of displacement of the two atoms. This bond is thus compressed only slightly (around 0.04 au). The situation is depicted in figure 6, which shows the distortion around the Fe impurity in the $(0, \bar{1}, 1)$ plane. The length of the arrows indicate roughly the relative amount of displacement. Not too surprisingly, we find a rather strong coupling between the displacement of the first two shells (those with non-zero driving forces) and the rest of the crystal in the sense that if all but the first two shells of atoms are kept in their undisturbed positions the first two shells relax only by about 2/3 of their unconstrained

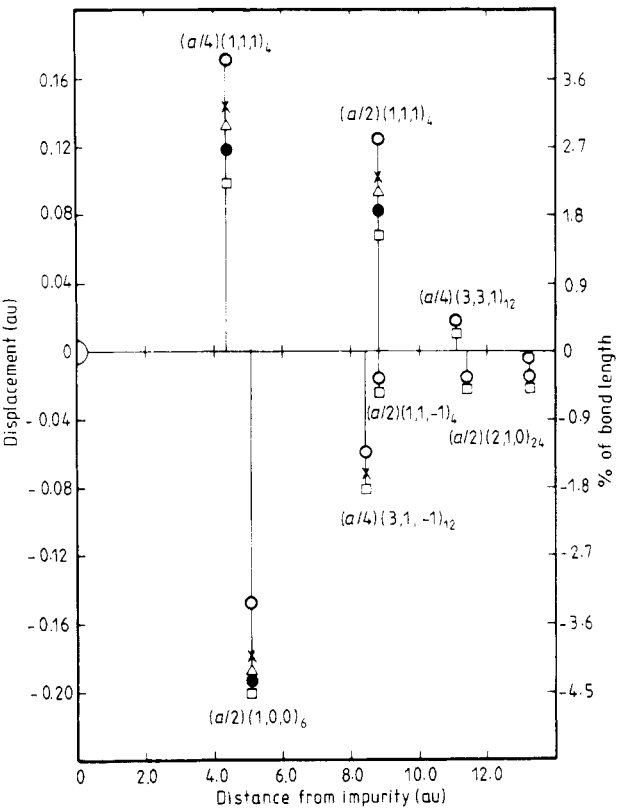

Figure 5. Displacement of the first nine shells of atoms around the TI position versus their distance from the impurity site in the undistorted lattice. The subscripts denote the number of atoms in a given shell and a is the lattice constant. ○ Ni, × Co, △ Fe, ● Mn, □ Cr.

relaxation. We note that the rather small but extended displacements are favourable to the present relaxation model. The small displacements make the basic approximation in the model less questionable, as discussed in § 2, while the extended nature of the distortion (four shells containing 26 atoms with non-negligible displacements) is treated simply and accurately by the VF model.

In order to find out what controls the driving force and hence the relaxation pattern, we examine the factors in the integrand in equation (13). Outside the core region, the host atom pseudopotential is the same as for a point charge. Inside the core, both $v_{ps}(r)$ and $dv_{ps}(r)/dr$ deviate substantially from the coulombic behaviour, owing to the kinetic energy versus potential energy cancellation effected by the pseudopotential. This is illustrated in figure 7 both for the 'soft' potential used here as well as for a 'hard-core' pseudopotential (Harris and Jones 1978). This non-coulombic behaviour describes the effect of an atomic core of finite dimension and leads to a pattern of relaxation which differs from that induced by point ions. The projected charge density $\boldsymbol{n}^{(p)}(r)$ around the pth host atom contains contributions both from the isotropic and anisotropic parts of $\Delta\rho(\boldsymbol{r})$. It is convenient to study first the contributions to $\boldsymbol{n}^{(p)}(r)$ from $\Delta\rho_0(r)$ only. Thus, excluding any contributions to the projected charge density perturbation from the

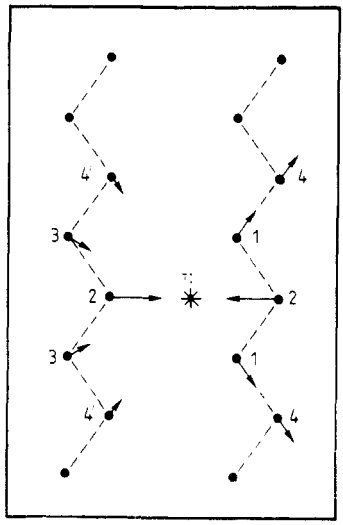

Figure 6. Schematic representation of the displacement of atoms in a $(0, \bar{1}, 1)$ plane. The length of the arrows indicate roughly the relative magnitudes of displacement of the different atoms (cf figure 5) and the integers denote the shell number in increasing distance from the Tl impurity.

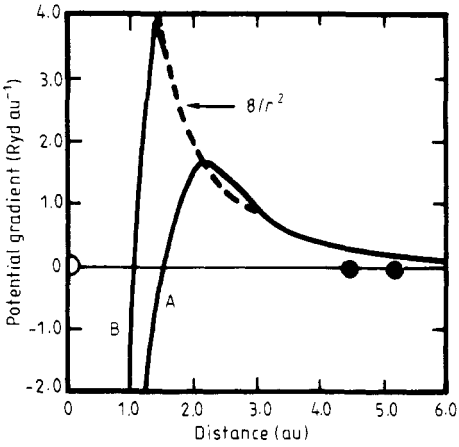

Figure 7. Radial derivative of the soft-core pseudopotential used here (curve A), of a hard-core pseudopotential (curve B) and of a point ion.

anisotropic parts of $\Delta\rho(\boldsymbol{r})$, we define the magnitudes

$$n_0^{(p=1)}(r) = -(4\pi)^{1/2}\Delta n^{(1)}_{1,t_2,x}(r) \tag{21a}$$

and

$$n_0^{(p=2)}(r) = -(4\pi/3)^{1/2}\Delta n^{(2)}_{1,t_2,x}(r) \tag{21b}$$

of the $l = 1$ projected charge density perturbation corresponding to the atoms at $(a/4)$ $(1,1,1)$ and $(a/2)$ $(1,0,0)$ (1NN and 2NN), respectively. These functions are plotted in figure 8 for Si : Fe. The notable feature of these curves is that the $l = 1$ projected density for the 1NN is positive for all values of r, whereas for the 2NN it starts out with a negative

value and becomes positive at around $r = 1.5$ au. It turns out that this feature controls the opposite displacements of the 1NN and the 2NN. In figure 9 we have plotted the integrand in equation (13) using the $l = 1$ projected density corresponding to the 1NN. For comparison we have also plotted the integrand using a point-ion potential (broken curve). The areas under these curves give the electronic force ΔF_e (the first term in equation (13)) acting on the respective host ion (i.e. pseudo- or point ion) in its undistorted 1NN position. The integral from the silicon core radius to infinity gives the same attractive contribution to the electronic force for the two potentials. Inside the silicon core, however, the contribution to the integral is seen to be less negative for the pseudo-ion than for the point ion. Adding the positive (repulsive) ion–ion interaction term ΔF_i (the second term in equation (13)), then, for the point ion, the negative (attractive) ΔF_e overwhelms the positive ΔF_i, resulting in a net inward relaxation, whereas for the pseudo-ion the less negative ΔF_e is overwhelmed by ΔF_i, producing a net *outward* relaxation. Since for the 2NN atoms the magnitude of the corresponding $l = 1$ projected density has a sign in the inner core region which is opposite to that for the 1NN, the non-coulombic behaviour in the pseudopotential will have just the opposite effect, i.e. increasing the attractiveness of ΔF_e, leading to an *inward* relaxation when balanced against ΔF_i. Thus, the opposite directions of relaxation for atoms in the 1NN and 2NN shells are dictated by the different behaviour in the $l = 1$ projected charge density perturbation in the silicon core region shown in figure 8.

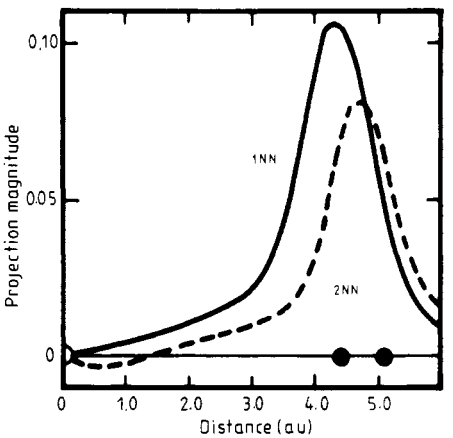

Figure 8. Magnitude of the projected density perturbation (equation (21)) for Si : Fe around the 1NN and 2NN atoms. The full circles represent the impurity atom seen from the 1NN and 2NN atoms.

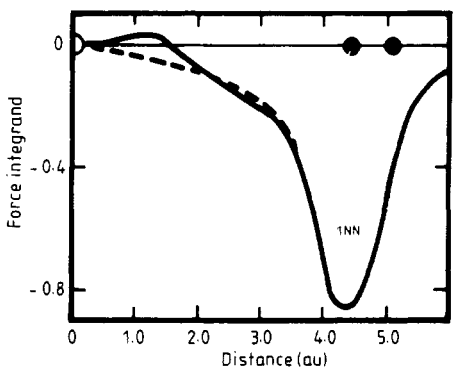

Figure 9. The integrand in equation (13) for Si : Fe around a 1NN atom when the host ion is represented by the pseudopotential (full curve) and by a point-ion potential (broken curve).

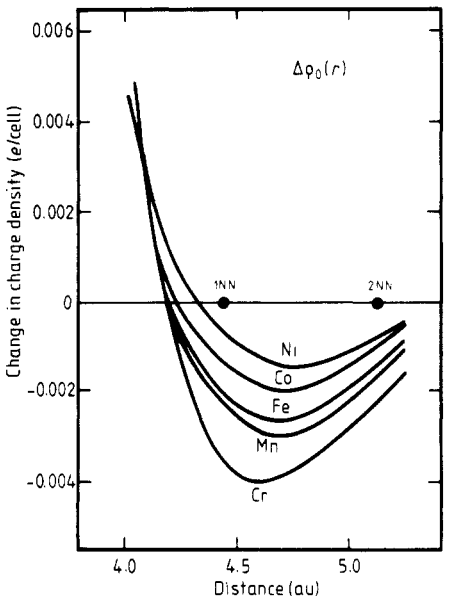

Figure 10. Chemical regularities in the spherically symmetric component of the impurity-induced change in charge density around the first- and second-nearest neighbour host atoms.

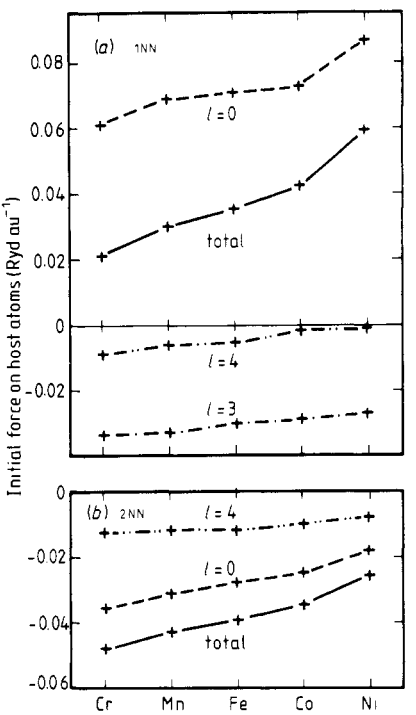

Figure 11. (*a*) The strength of the initial forces on the 1NN atoms for the various impurities (total) together with the contribution to the initial forces from the different l components in $\Delta\rho(r)$. (*b*) Same as in (*a*) but for the 2NN atoms.

To see how the details in the $l = 1$ projected density inside the silicon core are related to details in $\Delta\rho_0(r)$, one can construct a simple model. In figure 10 we show $\Delta\rho_0(r)$ for the different impurities in the neighbourhood of the 1NN and 2NN. The $l = 1$ projected densities are just these functions viewed from the respective atomic sites, retaining only the $l = 1$ component (equations (10)–(12)). If we approximate the negative portion of

a curve in figure 10 by a parabola, the $l = 1$ projected density magnitude $n_0^{(p)}(r)$ can be calculated analytically. We find that for small r, $n_0^{(p)}(r) = \alpha r$ where $\alpha > 0$ if the atom is situated to the left of the minimum of the parabola and $\alpha < 0$ otherwise. For larger r, $n_0^{(p)}(r)$ must become positive because of the positive peak in $\Delta\rho_0(r)$. But we have just seen how a positive (negative) value of α tends to favour an outward (inward) relaxation. In this way it is seen how the direction of relaxation is determined by the position of the atoms in the antibonding (negative) part of $\Delta\rho_0(r)$, as well as by the non-coulombic behaviour of the pseudopotential, and how the chemical trends in figure 5 are reflected into the relaxation pattern in figure 10: the heaviest impurity (Ni) induces the largest outward displacement of the 1NN but the smallest inward displacement of the 2NN, whereas the lightest impurity (Cr) does just the opposite. These trends reflect the fact that in going from Cr to Ni the bonding area increases in magnitude, whereas the antibonding area in figure 10 decreases. Although these considerations concern only the initial forces (which determine the direction of distortion), we expect them to be approximately correct also for the forces acting on slightly distorted atoms, simply because the antibonding structure in $\Delta\rho_0(r)$ extends on a length scale which rather much exceeds that of the calculated displacements.

In order to see the effects of the anisotropic charge rearrangement left out from the analysis so far, we show in figure 11 separately the contributions to the initial driving forces on 1NN and 2NN from the isotropic and anisotropic components in $\Delta\rho(r)$. For both shells the anisotropic parts of $\Delta\rho(r)$ give rise to forces which tend to pull the neighbouring atoms closer to the impurity. This contribution is, however, not strong enough to change the direction of distortion for the 1NN. In contrast, substitutional transition atom impurities reduce (weaken) the existing bonds (Zunger and Lindefelt 1983) leading to an overall outward relaxation of the lattice (Lindefelt 1983).

Acknowledgments

One of us (AZ) acknowledges support by the office of Energy Research, Materials Science Division, US Department of Energy, under grant No DE-AC02-77-CH00178. U Lindefelt acknowledges financial support from the Swedish Natural Science Research Council.

References

Deb B M 1973 *Rev. Mod. Phys.* **45** 22
Harris J and Jones R O 1978 *Phys. Rev. Lett.* **41** 191
Harris J, Jones R O and Müller J E 1981 *J. Chem. Phys.* **75** 3904
Kaufmann U and Schneider J 1980 *Festkörperprobleme, Advances in Solid State Physics* vol. 20, ed. J Treusch (Braunschweig: Vieweg) p 87
Larkins F P and Stoneham A M 1971a *J. Phys. C: Solid State Phys.* **4** 143
—— 1971b *J. Phys. C: Solid State Phys.* **4** 154
Lindefelt U 1983 *Phys. Rev.* B **28** 4510
Lindefelt U and Zunger A 1982 *Phys. Rev.* B **26** 846
—— 1984 *Phys. Rev.* B **30** 1102
Louie S G, Schlüter M, Chelikowsky J R and Cohen M L 1976 *Phys. Rev.* B **13** 1654
Ludwig G W and Woodbury H H 1962 *Solid State Physics* vol. 13, ed. H Ehrenreich, F Seitz and D Turnbull (New York: Academic Press) p 223
Solbrig A W Jr 1971 *J. Phys. Chem. Solids* **32** 77

Stoneham A M 1982 *Computer Simulation in Solids*, ed. C R A Catlow and W C Mackrodt (Berlin: Springer)
Weber E R 1983 *Appl. Phys.* A **30** 1
Wells A F 1975 *Structural Inorganic Chemistry* 4th edn (Oxford: Clarendon) p 789
Zunger A and Cohen M L 1978 *Phys. Rev.* B **18** 5449
—— 1979 *Phys. Rev.* B **20** 4082
Zunger A and Lindefelt U 1982 *Phys. Rev.* B **26** 5989
—— 1983 *Phys. Rev.* B **27** 1191